ATMOSPHERIC PRE-CORRECTED DIFFERENTIAL ABSORPTION TECHNIQUE TO RETRIEVE COLUMNAR WATER VAPOR [1]

Daniel Schläpfer[1], Christoph C. Borel[2], Johannes Keller[3] and Klaus I. Itten[4]

[1] permanent address: Department of Geography, RSL, University of Zürich, CH-8057 Zürich, Switzerland
Phone: +41 1 257 52 49, Fax: +41 1 362 52 27, E-mail: dschlapf@rsl.geogr.unizh.ch

[2] Los Alamos National Laboratory, NIS-2, MS C323, Los Alamos, NM 87545, USA

[3] Paul Scherrer Institut (PSI), CH-5232 Villigen PSI, Switzerland

[4] Remote Sensing Laboratories (RSL), Department of Geography, University of Zürich, CH-8057 Zürich, Switzerland

Abstract

Imaging spectrometry has the potential of remotely detecting atmospheric water vapor and other trace gases on the basis of their absorption of radiation. Water vapor has strong absorption features in the near infrared, which are used to retrieve its columnar content by differential absorption techniques. A new atmospheric pre-corrected Differential Absorption (APDA) technique is derived directly from simplified radiative transfer equations. It corrects for the atmospheric path radiance term in order to avoid mis-quantifications over dark background albedos. The comparison to traditional techniques shows the error reducing advantage of the new technique. A quantitative procedure of channel selection and method optimization and its implementation is shown. The application of the optimized method to AVIRIS images acquired in 1991 and 1995 results in estimates of the columnar water vapor within an accuracy of ± 5%.

1 INTRODUCTION

Water vapor is one of the main forces for weather development as well as for mesoscale air transport processes. The monitoring of water vapor is therefore an important aim in remote sensing of the atmosphere. Current operational systems for water vapor detection use primarily the emission in the thermal infrared (AVHRR, GOES, ATSR, Meteosat) or in the microwave radiation bands (DMSP). The disadvantage of current satellite systems is either a coarse spatial (horizontal) resolution ranging from one to tens of kilometers or a limited penetration into the lower atmosphere. Imaging spectrometry, on the other hand, measures total column water vapor contents at a high spatial horizontal resolution and has therefore the potential of filling these gaps.

The sensors of the AVIRIS instrument are capable of acquiring hyperspectral data in 224 bands located in the visible and near infrared at 10 nm resolution. This data includes the information on constituents of the earth's surface as well as of the atmosphere. The optical measurement of water vapor can be performed using sensor channels located in bands or lines of the absorption spectrum. The AVIRIS sensor has been used to retrieve water vapor and, with less accuracy, carbon dioxide, oxygen and ozone. To retrieve the water vapor amount, the so-called differential absorption technique has been applied (Carrère et al., 1993; Kaufman et al., 1992). The goal of this technique is to eliminate background factors by taking a ratio between channels within the absorption band and others besides the band. Various ratioing methods on the basis of different channels and calculation techniques were developed.

The influence of a trace gas of interest on the radiance at the sensor level is usually simulated by using radiative transfer codes. In this study, the spectral transmittance and radiance are calculated by MODTRAN3 simulations with the new DISORT option (Abreu et al., 1995). The objective of this work is to test the best performing differential absorption techniques for imaging spectrometry of tropospheric water vapor.

[1] submitted for publication to 'Remote Sensing of Environment' on March 4th, 1996

Name:	**Narrow Wide Technique**	**Continuum Interpolated Band Ratio**	**Linear Regression Ratio**
Shortcut:	N/W	CIBR	LIRR
Figure :	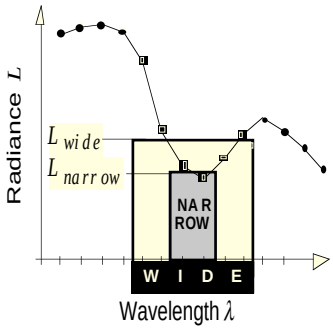	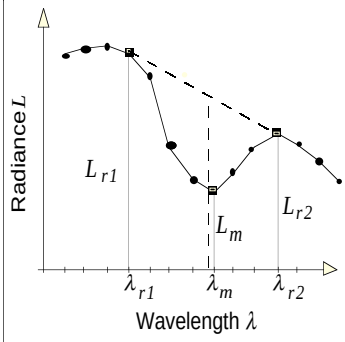	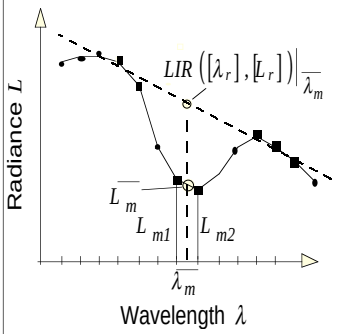
Equation:	$R_{N/W} = \frac{L_{narrow}}{L_{wide}}$	$R_{CIBR} = \frac{L_m}{\omega_{r1} \cdot L_{r1} + \omega_{r2} \cdot L_{r2}}$	$R_{LIRR} = \frac{\overline{L_m}}{LIR([\lambda_r],[L_r])\|_{\overline{\lambda_m}}}$
Parameters:	L_{narrow}: (averaged) radiance in a narrow measurement band L_{wide}: (averaged) radiance in a wide band at the same central wavelength as L_{narrow}	$\omega_{r1} = \frac{\lambda_{r2} - \lambda_m}{\lambda_{r2} - \lambda_{r1}}$ $\omega_{r2} = \frac{\lambda_{r1} - \lambda_m}{\lambda_{r2} - \lambda_{r1}}$	$\overline{L_m}$: mean radiance of all measurement channels; *LIR(x,y)*: linear regression line through points (x,y)
# Ref.-ch:	1 (includes mesurement area)	exactly 2	at least 3
# M.-ch:	1	exactly 1	at least 1
Source:	Frouin, 1989	Bruegge, 1990	Schläpfer, 1996
remarks	multispectral approach, in the hyperspectral case the channel sets are averaged	often used water vapor retrieval technique of high computational speed	extended CIBR technique, reduces total noise of the sensor

Table 1: Summarizing of differential absorption techniques, used for the water vapor retrieval

2 SUMMARIZING OF DIFFERENTIAL ABSORPTION TECHNIQUES

Differential absorption (DA) techniques are a practicable way to determine trace gas contents from a spectrum of an absorption band, which are easy to implement at low computing time costs. In general they perform a ratioing between channels within the absorption feature (measurement channels) and channels in its vicinity (reference channels) to detect the relative strength of absorption. Two major DA techniques were used for hyperspectral imaging spectrometry and compared by Carrère et al. (1993): The Narrow/Wide technique (Frouin et al., 1990) and the Continuum Interpolated Band Ratio (Bruegge et al., 1990). A third technique, the Linear Interpolated regression ratio was introduced by Schläpfer et al. (1996). Curve fitting techniques (Gao and Goetz, 1990a) are not considered in this study, because of their higher complexity and computing time. Table 1 shows a summarizing compilation of the three mentioned techniques.

3 DERIVATION OF THE ATMOSPHERIC PRE-CORRECTED DIFFERENTIAL ABSORPTION TECHNIQUE (APDA)

Duntley in 1948 (see Middleton, 1952) expressed the radiance L measured in one specific channel by a sensor as:

$$L \;=\; \rho\,\frac{1}{\pi}E_0\;T_{tot} \;+\; L_{hor}(1-T^*), \tag{1}$$

where E_0 is the extraterrestrial solar irradiance, T_{tot} is the total transmittance of the earth's atmosphere, L_{hor} is the radiance one would measure in a plane parallel atmosphere in horizontal direction and T^* is the corresponding special transmission term (Duntley assumes: $T_{tot} = T^*$). The apparent ground reflectance ρ includes the reflectance of the observed pixel as well as of the adjacent area (adjacency effects). It therefore never can get to zero in reality. All the parameters of equation (1) are dependent on the central wavelength of the used channel.

The total transmittance is now split into the water vapor transmittance T_{wv} and a residual transmittance T_0, which depends on aerosols and gas absorptions. The second term in 1 is the backscattered atmospheric path radiance not reflected by the ground ($L_{atm} = L_{hor}(1-T^*)$), as parametrized by Duntley. The radiance at the sensor level L can now be expressed in a simple form as:

$$L \;=\; \rho\;E_0\;T_0\;T_{wv} + L_{atm} \;=\; L_{gnd}\,T_{wv} \;+\; L_{atm} \tag{2}$$

where $L_{gnd} = \rho E_0 T_0$ is the total ground reflected radiance at the sensor level, if no water vapor were present. L_{atm} is not dependent on the ground reflectance ρ but is sensitive to the atmospheric composition, in particular to the aerosol amount and the water vapor content. These latter values depend on the ground altitude h.

Using this equation we first write the radiances in three channels $i = m,\ r1$ and $r2$ where m is a measurement channel in an absorption region, e.g. the 940 nm water vapor absorption, and $r1$ and $r2$ are two reference channels. The transmittance $T_{wv,m}$ is a function of water vapor for channel m but not for the reference channels $r1$ and $r2$. Assuming a small difference between the central wavelengths λ_{r1} and λ_{r2} of the reference channels and $\lambda_{r1} < \lambda_m < \lambda_{r2}$ the radiance in a measurement channel L_m can be approximated by a linear interpolation as:

$$L_m = [w_{r1}L_{gnd,r1} + w_{r2}L_{gnd,r2}]\;T_{wv,m} \;+\; L_{atm,m}, \tag{3}$$

where

$$w_{r1} = \frac{\lambda_{r2} - \lambda_m}{\lambda_{r2} - \lambda_{r1}} \quad \text{and} \quad w_{r2} = \frac{\lambda_m - \lambda_{r1}}{\lambda_{r2} - \lambda_{r1}}. \tag{4}$$

Note that we assume the reference channels have no water vapor absorption, i.e. $T_{wv,r1} = 1$ and $T_{wv,r2} = 1$. Solving equation (3) for the transmittance in the water vapor channel $T_{wv,m}$ and substituting $L_{gnd,r1}$ and $L_{gnd,r2}$ from equation (2) we find an equation similar to the CIBR (see table 1) but with pre-correction terms for the atmospheric path radiances $L_{atm,i}$:

$$T_{wv,m} = \frac{L_m - L_{atm,m}}{w_{r1}(L_{r1} - L_{atm,r1}) + w_{r2}(L_{r2} - L_{atm,r2})} \tag{5}$$

At low ground reflectance, the atmospheric radiance is the major contributor to the total radiance, whereas at higher reflectance the ground reflected radiance term dominates. The CIBR equation (see table 1) is based on the assumption, that the atmospheric path radiance is neglectable against the ground reflected radiance. When we introduce the total radiance following equation (2) and assume that the ground reflectance ρ is very low, the original CIBR equation reduces to:

$$R_{CIBR}(\rho_{g,i} \approx 0) \;\approx\; \frac{L_{atm,m}}{w_{r1}L_{atm,r1} + w_{r2}L_{atm,r2}}. \tag{6}$$

Since $L_{atm,r1}$ and $L_{atm,r2}$ are nearly independent on the water vapor contents, the CIBR is then proportional to the water vapor-dependent atmospheric path radiance $L_{atm,m} = L_{h,m}[1 - T^*_m]$ which is no longer proportional to $T_{wv,m}$. When the background reflectance is high, the CIBR equation reduces to:

$$R_{CIBR}(\rho_{g,i} \approx 1) \;\approx\; Const\; T_{wv,m}. \tag{7}$$

Thus the CIBR is proportional to $T_{wv,m}$ only for high background reflectances. At low background reflectances the water vapor retrieval gets less accurate, resulting in an obvious underestimation over dark surfaces (Gao and Geotz, 1990a). For an improved water vapor retrieval it is therefore necessary to apply the derived APDA technique instead of the CIBR.

The atmospheric pre-correction term $L_{atm,i}$ is a function of terrain height, channel position and water vapor contents. It can be estimated by simulating the total radiance at the sensor at zero albedo under varying ground altitude and water vapor contents. To increaase the accuracy an iterative approach is necessary, taking the first estimate of the path radiance from the image.

In this derivation only one measurement and two reference channels were used. However, equation (5) can also be extended to more channels, analogous to the linear regression ratio, given in table 1. The linear interpolation of two reference channels is replaced by a linear regression line through an arbitrary number of channels and evaluated at the center wavelength of the measurement channels. The radiance values L_i of each channel i are reduced by the corresponding atmospheric path radiance terms $L_{atm,i}$ and inserted in the LIRR equation. This equation is the common APDA equation which reduces directly to equation (5) for the three channel case:

$$R_{APDA} = \frac{\overline{[L_m - L_{atm,m}]_i}}{LIR\left([\lambda_r]_j\,, [L_r - L_{atm,r}]_j\right)\Big|_{\overline{[\lambda_m]_i}}} \tag{8}$$

where $LIR([x],[y])|_a$ is a linear regression line through the points (x, y) evaluated for y at the point $x = a$. The parameters in brackets are vectors of i measurement channels and j reference channels respectively.

4 COMPARISON OF CIBR AND APDA RATIOS ON SIMULATED DATA

4.1 Comparisons of the CIBR and APDA Ratios for a Fixed Water Vapor Amount

To test the APDA equation (5) and the CIBR (see table 1) the irradiance, transmittance and path radiance was computed with MODTRAN3, using the DISORT option. The atmospheric state was mid-latitude summer, visibility of 23 km and the columnar water vapor was fixed at 2.4 g/cm^2. The target height was at 0.4 km, the sun at 40 degrees with approximately 1 nm spectral resolution. The ground reflectances ρ_{r1} and ρ_{r2} were changed from 0.05 to 1.0 in steps of 0.05 on both sides of the spectral range $(\lambda_{min(r1)}, \lambda_{max(r2)})$ which is defined as the minimum and maximum wavelengths of channels r1 and r2. The following formula is used to create the various reflectance background spectra:

$$\rho(\lambda) = \rho_{r1} + \frac{\rho_{r2} - \rho_{r1}}{\lambda_{max(r2)} - \lambda_{min(r1)}}\lambda - \lambda_{min(r1)}. \tag{9}$$

The selected optimum AVIRIS bands (55, 62 and 68) for 1995 data have the following full-width-half-maximum $r1$: 0.869-0.879 μm, m: 0.936-0.946 μm and $r2$: 0.994-1.004 μm (see section 5). The simulation results show, that the APDA is less sensitive to reflectance variations than the CIBR (see figure 1).

Using broader bands, e.g. in a future multispectral sensor such as MODIS, similar results are achieved. The selected bands are $r1$: 0.86-0.89 μm, m: 0.91-0.97 μm and $r2$: 0.99-1.04 μm. Figure 1 shows a scatterplot of all computed CIBR and APDA ratios as a function of the band-averaged reflectance in channel 2. Note the large range for the CIBR compared with the APDA techniques. Also the CIBR maps low reflectances ($\rho_m < 0.2$) to higher ratios, whereas the APDA maps all reflectances to an almost constant ratio. There is still a residual effect visible from reflectance slopes (markers forming lines with positive slopes) which could be corrected as well. The influence of reflectance slopes is similar for the CIBR and the APDA. The ratios

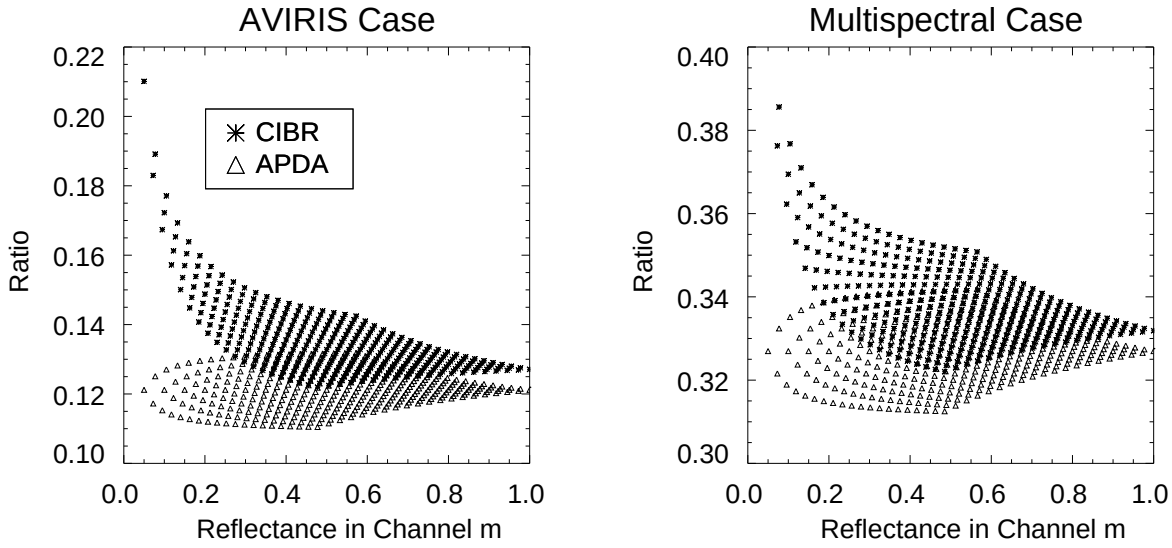

Figure 1: Water vapor ratios as a function of band-averaged ground reflectance of channel 2 for a 10 nm bandwidth instrument (AVIRIS) and a multispectral instrument (e.g. MODIS) using Duntley's model.

or quasi water vapor transmittances for the AVIRIS case are much lower than for the multispectral case because the thinner AVIRIS measurement channel has a lower overall transmittance in the deep water vapor absorption feature.

Note that we have not yet investigated how the APDA technique depends on atmospheric conditions (aerosol loading, etc), calibration errors and radiative transfer code uncertainties.

4.2 Comparisons of the CIBR and APDA Ratios for Variable Water Vapor and 379 Reflectance Spectra

The behavior of CIBR and APDA techniques over spectrally varying background was tested by another simulation. Existing reflectance spectral data bases for 165 (Grove et al, 1992) and 25 (Kruse et al, 1992) minerals and 64 other spectra of natural and man-made materials were used as background. Since leaves contain significant amounts of water, a data base for 125 simulated leaf reflectance and transmittance spectra with variable leaf water content (0.0046 to 0.0405 cm) was created using the PROSPECT REDUX model (Jacquemoud et al, 1995). The radiosity method was then used to compute canopy spectra of a 20-layer canopy with a total leaf area index (LAI) of 5 (Borel et al, 1990).

All 379 reflectance spectra were resampled at 2.5 nm spacings. The radiative transfer code 6S (Vermote et al, 1994) was used to compute the TOA radiance over the water vapor band centered on 940 nm. The water vapor amounts ranged from 0.05 to 5 g/cm^2 in 12 steps. The atmosphere had a visibility of 20 km with continental aerosols. The target height was set at sea level and the sensor located above the atmosphere. Only the data for water vapor amounts ≥ 1 g/cm^2 was used in the following analysis. Figure 2 shows the RMS relative error in percent:

$$\varepsilon(PW_j) = 100\sqrt{\frac{1}{N}\sum_{i=1}^{N}[\frac{(PW_{j,true} - PW_{i,est})}{PW_{j,true}}]^2}$$

in water vapor for all N =379 reflectance spectra as a function of water vapor. The four different techniques are:

1. **CIBR**: Original CIBR equation (see table 1).

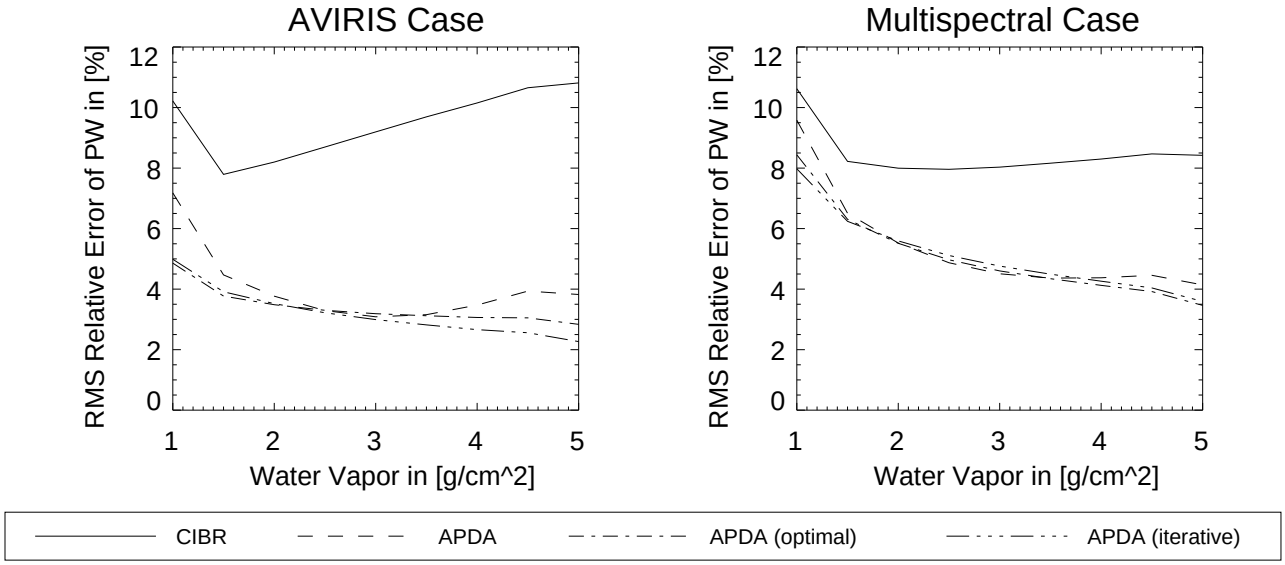

Figure 2: RMS relative error $\varepsilon(PW_j)$ in % of water vapor for all 379 reflectance spectra as a function of water vapor for four different water vapor retrieval techniques.

2. **APDA**: Regular APDA equation (5) using a fixed water vapor amount of 3 g/cm^2 to compute the atmospheric path radiance $L_{atm,m}$.

3. **APDA (optimal)**: Equation (5) with computed water vapor-dependent atmospheric path radiance $L_{atm,m}(PW)$.

4. **APDA (iterative)**: Equation (5) with the iterative scheme described in section 6, figure 5.

The various water vapor retrieval techniques were compared by a measure similar to a quasi signal to noise ratio (SNR):

$$SNR(R_x(PW)) = \frac{\overline{R}_x(PW_{min})) - \overline{R}_x(PW_{max})}{\sigma(R_x(PW))}, \text{ where } x = \{\text{CIBR}, \text{APDA}, \text{APDA(opt.)}, \text{APDA(it.)}\}, \tag{10}$$

where $PW_{min} = 1\ g/cm^2$ and $PW_{max} = 5\ g/cm^2$ are the minimum and maximum water vapor contents, $\overline{R_x(PW)}$ denotes the average over $R_x(PW)$, $\sigma(R_x(PW))$ denotes the standard deviation over $R_x(PW)$. Table 2 shows the minimum and maximum SNR for four retrieval techniques.

Case:	AVIRIS			Multispectral		
Retrieval Technique	Range of R	$\overline{\sigma(R)}$	$SNR_{min/max}$	Range of R	$\overline{\sigma(R)}$	$SNR_{min/max}$
CIBR	0.243	0.01607	14.7-15.8	0.267	0.01511	16.7-17.9
APDA	0.253	0.00604	21.5-58.7	0.277	0.00870	18.4-42.1
APDA (optimal)	0.245	0.00496	30.5-66.8	0.267	0.00789	20.7-50.2
APDA (iterative)	0.246	0.00497	30.5-66.6	0.270	0.00796	21.2-49.7

Table 2: SNR comparison of four water vapor retrieval techniques. R and $\sigma(R)$ are unit free ratio numbers.

Next we compare the retrieval methods by setting thresholds at $\pm 5\%$ and $\pm 10\%$ RMS relative water vapor and counting the number of spectra which indicates how robust the retrievals are over many different

backgrounds. Table 3 summarizes the results obtained for all 379 background spectra using the four above described techniques:

Retrieval Technique	AVIRIS 5%	Multispectral 5%	AVIRIS 10%	Multispectral 10%
CIBR	35.3562	32.9815	9.49868	13.1926
APDA	8.17942	21.1082	1.84697	3.16623
APDA (optimal)	8.70712	20.3166	2.37467	3.43008
APDA (iterative)	7.91557	20.3166	1.84697	3.16623

Table 3: Percentage of reflectance spectra above 5% and 10% RMS Relative Water Vapor Error

Figure 3 shows a scatterplot of the relative water vapor errors over 379 backgrounds as a function of band-averaged ground reflectance. The CIBR has large water vapor errors for low ground reflectance and the regular and iterative APDA work better at low reflectance levels. The AVIRIS case has fewer reflectance spectra above the $\pm$ 10% limit than the multispectral approach, as is also evident from table 3. In both scatterplots the simulated vegetation spectra show up as two clustered sets of points along two lines between reflectances 0.55 and 0.66. The water vapor error is negative because vegetation has a water absorption feature which increases the apparent water vapor in the atmosphere causing a negative error in the estimated atmospheric water vapor. This feature could potentially be exploited to estimate canopy water content (Gao and Goetz, 1990b). Some of the materials in which the iterative APDA had relative water vapor errors of more than $\pm$ 10% are listed below in table 4.

AVIRIS-Case:	
CUMMINGTONITE-IN-6A (sloped) (non-linear)	ENSTATITE-IN-10B (sloped) (non-linear)
FAYALITE-NS-1A (dark) (sloped) (non-linear)	HEMATITE-FE2602 (sloped) (non-linear)
MOLYBDENITE-S-11A (sloped)	SIDERITE-COS2002 (sloped) (non-linear)
TRIPHYLITE-P-4A (sloped)	
Multispectral Case:	
ANTHOPHYLLITE-IN-8A (non-linear)	ANTLERITE-SO-11A (sloped) (non-linear)
BUDDINGTONITE-NHB2301	CUMMINGTONITE-IN-6A (sloped) (non-linear)
DICKITE-PS-3A (dark) (sloped) (non-linear)	ENSTATITE-IN-10B (sloped) (non-linear)
FAYALITE-NS-1A (dark) (sloped) (non-linear)	HEMATITE-FE2602 (sloped) (non-linear)
MOLYBDENITE-S-11A (sloped)	SIDERITE-COS2002 (sloped) (non-linear)
TOURMALINE-DRAVITE-S-CS-1A (dark) (sloped) (non-linear)	
TRIPHYLITE-P-4A (sloped)	

Table 4: Materials with RMS Relative Water Vapor Errors $>$ 10% for AVIRIS Case and Multispectral Case

A spectrum was classified as 'dark' if the average reflectance in channel m was below 0.1. A spectrum was considered 'sloped' if the absolute of the normalized difference

$$R_{slope} = \frac{|\overline{\rho_{r1}} - \overline{\rho_{r2}}|}{\overline{\rho_{r1}} + \overline{\rho_{r2}}}$$

between the channel averaged reflectances of channels $r1$ and $r2$ exceeded 0.05. A spectrum was considered 'non-linear' if the ratio $R_{non-linear}$ was less than 0.95 or greater than 1.05:

$$R_{non-linear} = \frac{\overline{\rho_m}}{w_{r1}\overline{\rho_{r1}} + w_{r2}\overline{\rho_{r2}}}$$

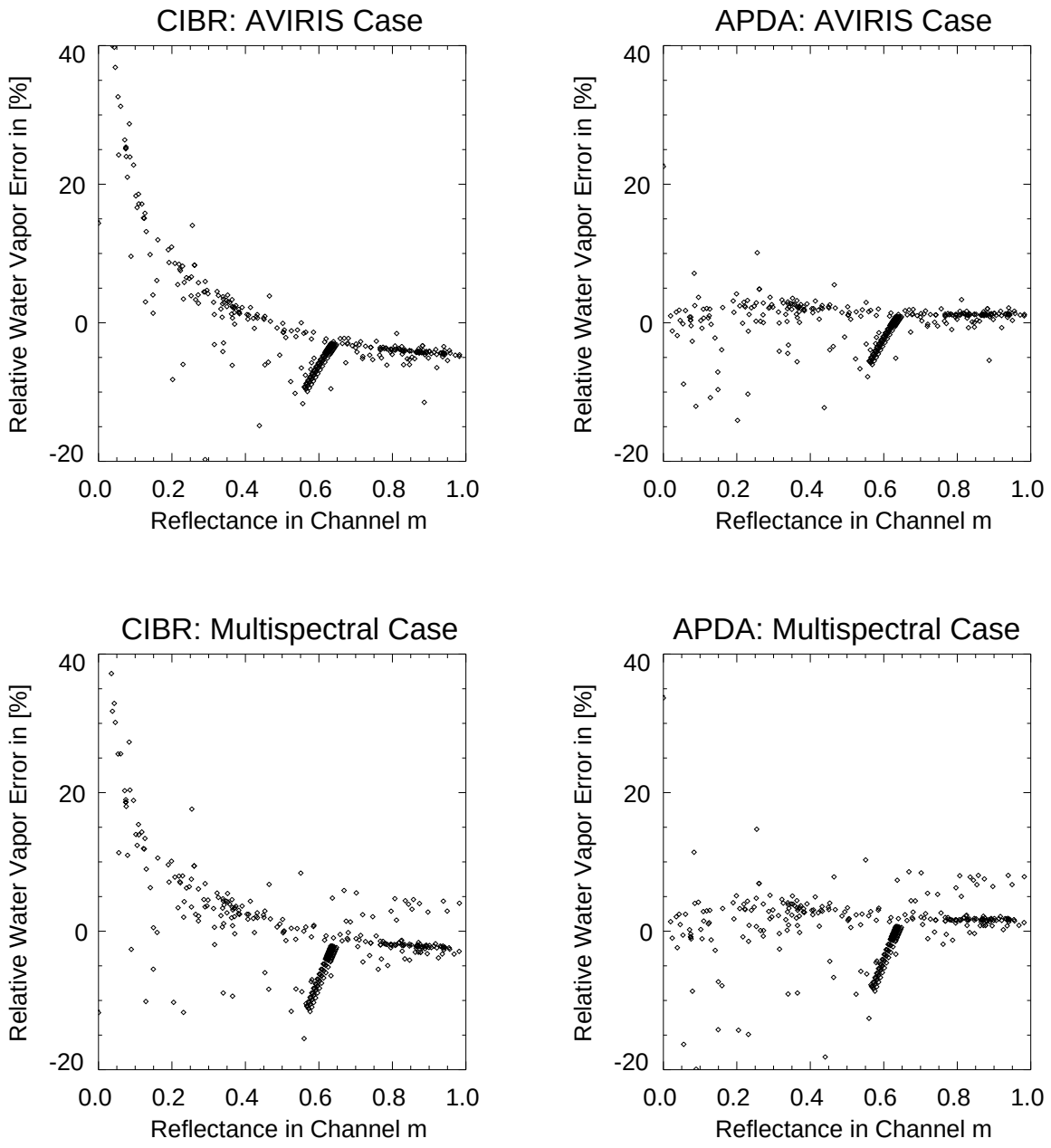

Figure 3: Relative water vapor errors over 379 backgrounds as a function of band-averaged ground reflectance for a 10 nm bandwidth instrument (AVIRIS) and a multispectral instrument. Note: The lined up points near 0.6 reflectance are from canopy spectra.

5 CHANNEL SELECTION

5.1 Evaluation of measurement channels

The two channel categories mentioned in section 2 are evaluated using the channel selection procedure proposed by Schläpfer et al. (1995a). Measurement channels are searched within the absorption band because they should be sensitive to variations of the trace gas amount. Furthermore the difference between the signal of the trace gas and the noise must be clearly discernible in these channels and other absorbing atmospheric species must not disturb the signal of the trace gas of interest. These three requirements are rewritten in mathematical form to get wavelength dependent qualifiers for each imaging spectrometer channel (Schläpfer, 1995). Their combination leads to a common evaluation equation for measurement channels:

$$M_{meas} \;=\; M_{sens}\; M_{sign}\; M_{cross} = [-e\; T_{wv}\; ln(T_{wv})] \left[\frac{(L_{s,0} - L_s) - \Delta L}{L_{s,0} - L_s}\right] [T_0], \tag{11}$$

where

$$\Delta L \;=\; \sqrt{(L_{ner})^2 + (L_{scal})^2 + \left(\frac{\Delta\rho}{\rho}\; L_{gnd}\right)^2} \tag{12}$$

The following parameters are simulated for the AVIRIS channel characteristics using the MODTRAN3 radiative transfer code: The water vapor transmittance T_{wv} , the total atmosperic transmittance T_0 of all the other absorbing atmospheric species, the radiance at the sensor level L_s, the total ground reflected radiance L_g and the radiance $L_{s,0}$ at the sensor level when no water vapor were present. ΔL is the effective total uncertainty observed at the sensor as described in equation 12, depending on three major parameters: The total noise equivalent radiance L_{ner} of the sensor channel (from the sensor specifications), the radiance error due to spectral calibration uncertainty L_{scal} and an estimate of the relative ground reflectance variation $\frac{\Delta\rho}{\rho}$ in a channel. The latter can be calculated as the channel dependent standard deviation deduced from various vegetation types of a spectral database. As an alternative, it can be derived from the mean standard deviation of each image channel relative to its average radiance.

5.2 Evaluation of reference channels

A reference channel has to meet two conditions: The signal should not be influenced by any atmospheric species and the effective signal to uncertainty (ΔL) ratio must be as big as possible. Analogous to equation 11 the channel qualifier for the reference channels is defined as the product of a transmittance factor M_{trans} and a radiance uncertainty factor M_{noise}. Introducing the expressions for the two factors yields the equation for the evaluation of reference channels:

$$M_{ref} \;=\; M_{trans}\; M_{noise} = [T_{wv}\; T_0] \left[\frac{L_s - \Delta L}{L_s}\right]. \tag{13}$$

	AVIRIS 1991 data	AVIRIS 1995 data
measurement channels	57,59 to 62 (910, 930 to 959 nm)	61 to 64 (932 - 961 nm)
reference channels	52 to 54 (862 to 881 nm)	54 to 56 (865 to 884 nm)
(near the selected meas.channels)	66 to 70 (987 to 1036 nm)	68 to 70 (999 - 1018 nm)

Table 5: Selected AVIRIS channels for 1991 and 1995 datasets.

In addition, the wavelength distance of the reference channels from their corresponding measurement channels has to be considered. That quantity has to be minimized to reduce errors due to non-linearity effects of the background radiance.

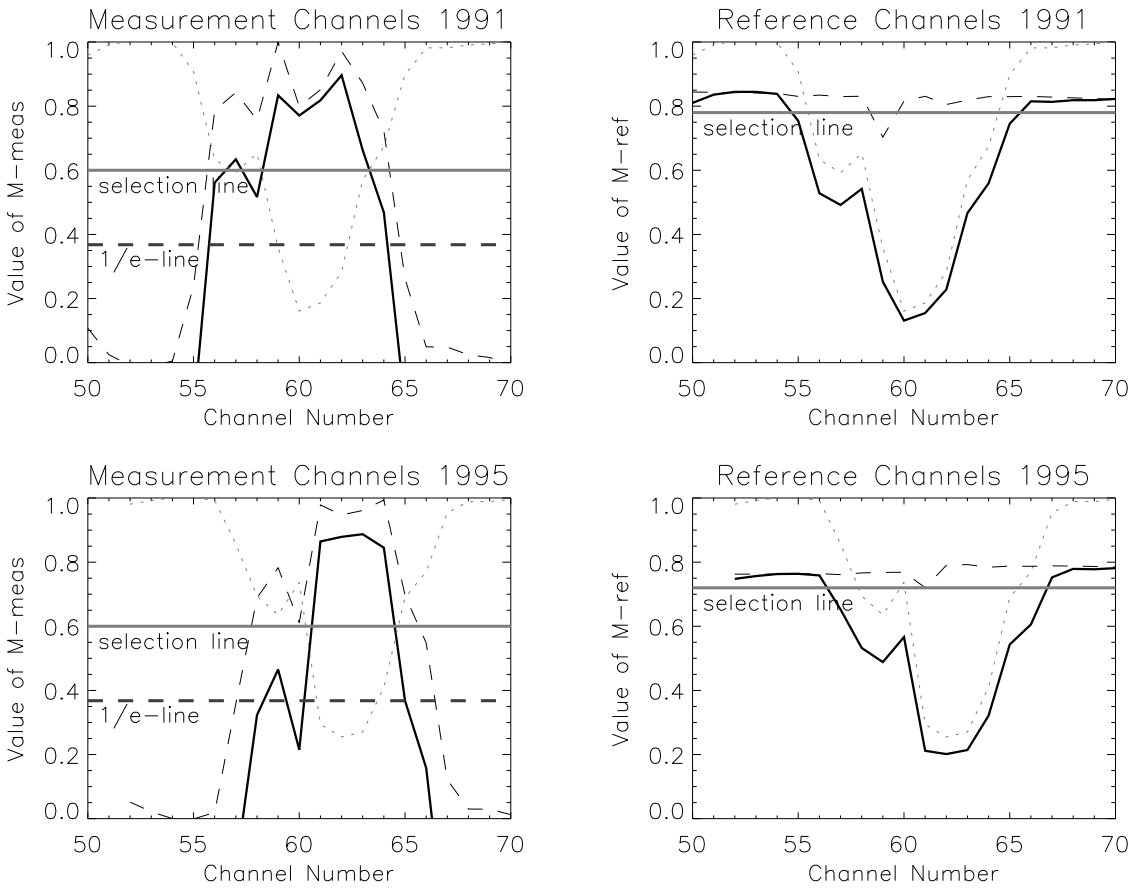

Figure 4: Channel qualification for AVIRIS 1991/1995 data in the 940 nm Absorption region. The dotted line is the total water vapor transmittance for both years, the thin dashed line is M_{sens} for measurement channels and M_{noise} for refer ence channels. The $\frac{1}{e}$-line indicates the optimal transmittance for measurement channels. Channels above the selection line were further considered for the method selection procedure.

5.3 Results for AVIRIS data

The channel selection procedure was applied to simulated data corresponding to AVIRIS images from 1991 over Central Switzerland and from 1995 over Camarillo (California). Ranked sets of channels to be used in differential absorption techniques were defined. A first analysis showed, that the best suited wavelength region for nadir viewing sensors under intermediate atmospheric conditions ($\approx$ 2-3 cm of precipitable water vapor) is the 940 nm absorption band. Hence, only channels between about 850 nm and 1070 nm were further considered (see table 5). At lower water vapor contents (below 1 cm), a stronger band with sufficient absorption may be considered, whereas at high contents the channels in the band slopes are favored.

A crucial factor for the channel selection is the total water vapor transmittance, which has to be estimated from an average total columnar water vapor content for each scene. It is integrated from radiosonde profiles, taken the day and time of the overflight and influences mainly the selection of the measurement channels. A plot of single factors, following the equations (11) and (13), for 1995 and 1991 AVIRIS channels is shown in figure 4. Table 5 lists the selected channels for the two datasets.

6 OPTIMIZATION OF THE APDA TECHNIQUE

6.1 Implementation of the APDA technique

The Differential Absorption technique itself only yields unquantified ratio values (corresponding to the trace gas transmittance), which have to be transformed to total water vapor amounts. Frouin et al. (1990) and Carrère et al. (1993) used an exponential approach for the correlation between the differential absorption ratio R and the corresponding water vapor amount (PW). For the present study this correlation was extended to an equation with three empirical regression paramters α, β and γ.

$$T_{wv} \approx R = e^{-\left(\gamma+\alpha(PW)^{\beta}\right)} \tag{14}$$

solved for the water vapor amount:

$$PW = -\left(\frac{ln(R)+\gamma}{\alpha}\right)^{\frac{1}{\beta}} \tag{15}$$

The following iterative procedure is used to compute the water vapor image (compare figure 5 for a flow chart of the whole APDA algorithm):

1. Use a radiative transfer code (6S or MODTRAN 3) to compute a Look Up Table (LUT) containing the total radiance at the sensor ($L_{s,i}$) for an average reflectance background (e.g. $\rho_{g,i} = 0.4$) and the atmospheric path radiance $L_{atm,i}$ as a function of water contents and terrain height.
2. Find the ratio values corresponding to the water vapor amounts of each MODTRAN3 run by applying the APDA technique to the LUT (subtract the path radiance term from the Total Radiance term and calculate ratio value).
3. Fit all the ratio values to the water vapor amounts using the function (15) and store the regression parameters α, β and γ.
4. Assume as starting value the average water vapor content given by the radiosonde profile for all image pixels and subtract the height dependent path radiance term from the image.
5. Calculate the APDA ratio following equation (8) and transform the ratio values to water vapor contents, using the quantification parameters and equation (15).
6. Substitute the values of $L_{atm,i}$ in equation (8) with the new water vapor dependent values, derived from the LUT.
7. Calculate the image ratio R_{APDA} a second time and transform the ratio values to the final water vapor contents $PW(image)$.

(8.) Repeat steps 5 and 6 a few times or until $|\overline{PW_i} - \overline{PW_{i-1}}| \leq 10^{-4}$.

Our computations have shown that it is sufficient to perform one iteration. Sometimes, the results even get worse after an increasing number of iterations, because errors may be amplified by this pixel based procedure. The regression parameters are retrieved only once at the begining of the calculation as best fitting for all simulated situations. This allows to decrease the computing time from nearly hours to less than one minute, the potential quantification errors being less than 1%. Typical values for α are 0.12- 0.18, for β: 0.65 to 0.80 and for γ: -0.05 to 0.4.

6.2 Optimization of the Channel Combination

In the following, the term 'method' is used for a differential absorption technique based on one specific channel combination set. A good method for the measurement of a trace gas must show little noise and background reflectance effects due to the total radiance uncertainty of the single channels (see equation (12)) and low cross sensitivity to variations of disturbing atmospheric constituents. The APDA technique given in section

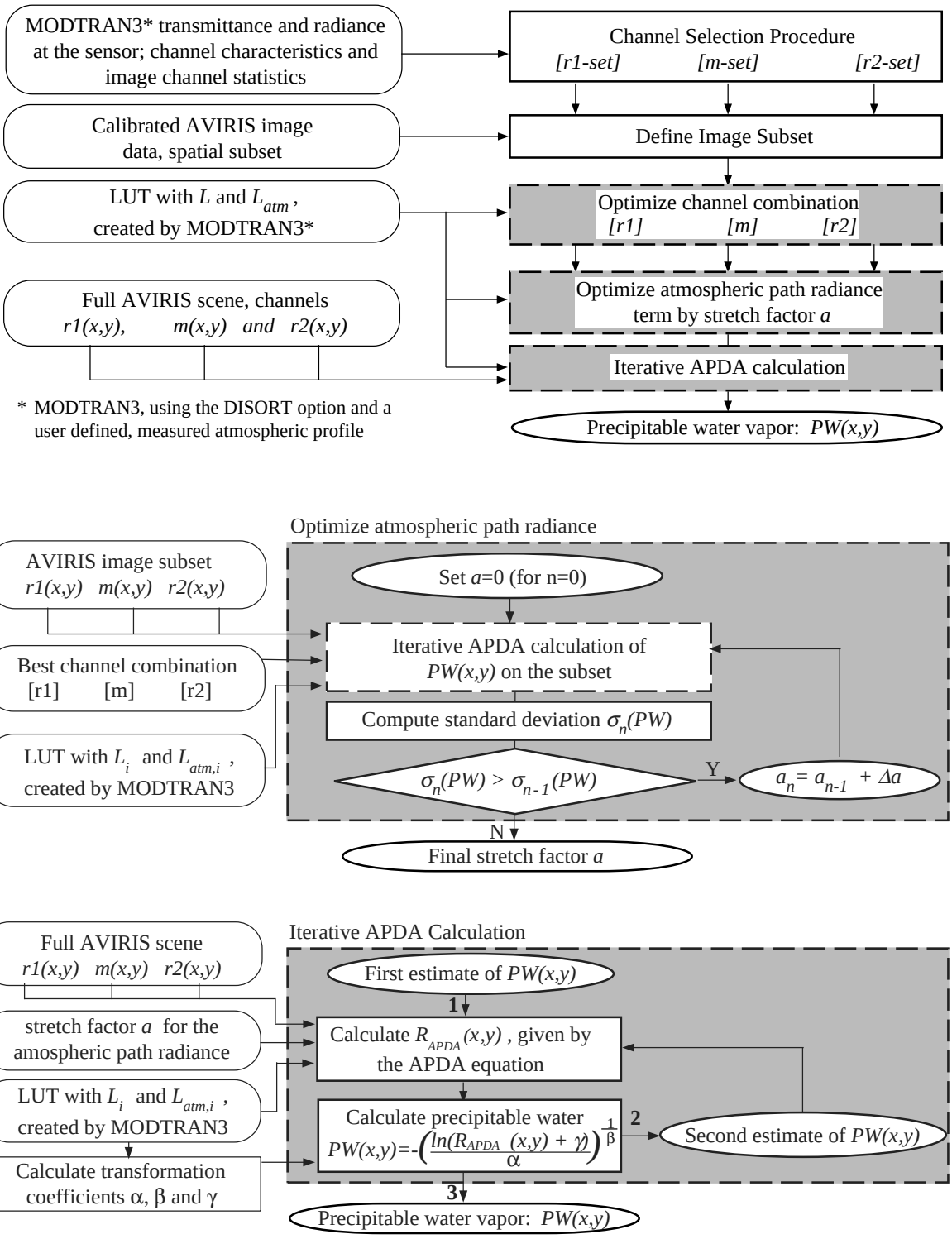

Figure 5: Flow chart of the whole APDA algorithm as implemented for application with AVIRIS images. Shaded boxes in the topmost main chart are displayed in separte charts below.

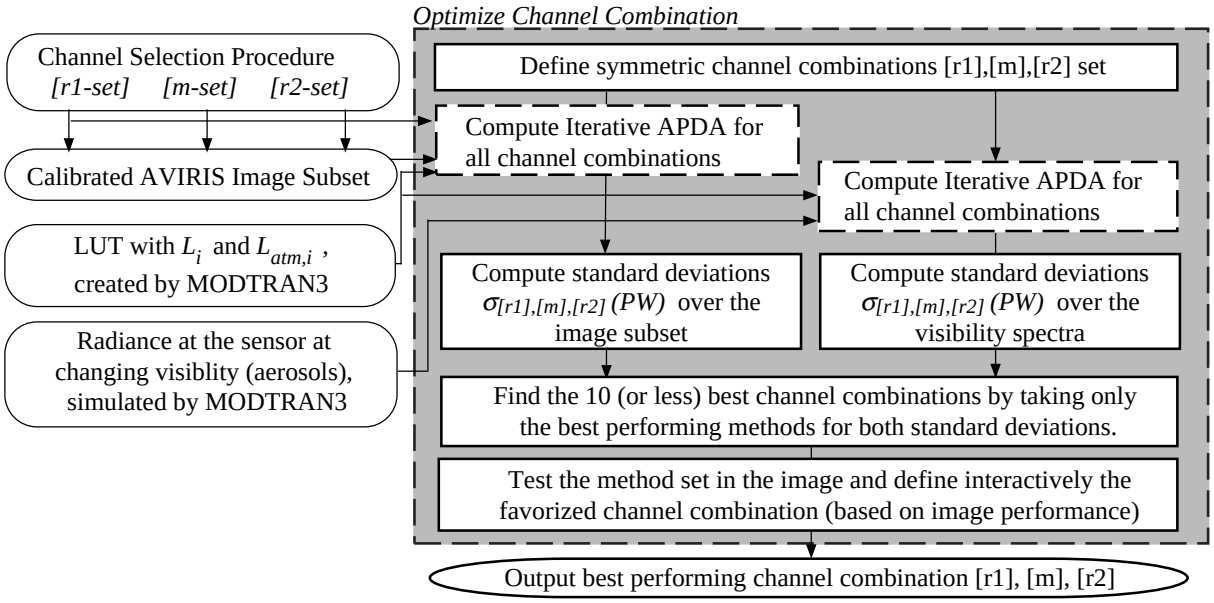

Figure 6: Flow chart of the algorithm to optimize the channel combination out of a given channel set from the selection procedure.

3 is applied for various channel combinations and tested regarding the above conditions. A qualifier for the noise and background effect is found based on the standard deviation of the quantified water vapor amount within an image subset ($\sigma(PW)_{sub}$). It is assumed that the effective water vapor signal($\sigma(PW_{wv})_{sub}$) and the uncertainty signal($\sigma(PW_{\Delta L})_{sub}$) overlay each other independently. Therefore the standard deviation of the water vapor contents over the subset and for each considered method is taken as qualifier value, which has to be minimal.

$$Q_{noise} = \sigma(PW)_{sub} = \sqrt{\sigma^2(PW_{wv})_{sub} + \sigma^2(PW_{\Delta L})_{sub}} \rightarrow MIN \tag{16}$$

The influence of aerosols is determined using MODTRAN3 simulations with constant water vapor amount but changing aerosol amounts (by introducing variations of the visibility). The standard deviation of the corresponding quantified water vapor amounts (PW_{vis}) of a number of visibility simulations is taken as a second qualifier for the method selection.

$$Q_{aerosol} = \sigma(PW_{vis}) \rightarrow MIN \tag{17}$$

Based on the selected channels, all possible combinations of APDA methods with 4 (respective 2) reference channels and 2 (respective 1) measurement channels are introduced and tested on the above qualifiers (compare flowchart in figure 6). For 1991 a set of 270 methods and for 1995 one of 108 methods was investigated. A limit for the qualifiers was set to get a pre-evaluated number of methods, which had to fulfill the requirements in the best 10 percent of all the methods. The percent limit was interactively reduced until less than 10 methods remained. These methods are applied to the whole images. Special effects in the resulting water vapor image, like erroneous channels or obvious misquantifications can lead to further exclusions and re-evaluation of other methods. This 'practical evaluation', based on effective quantification results, ground truth comparisons and effects in the resulting image is a second step of the method selection process, which shall not be neglected.

In general, the main influence on the absolute water vapor retrieval comes from the chosen measurement channels. The effects of the measurement channel position for 1991 and 1995 data is shown in figure 7. In both datasets the measurement channels 59 and 61 respectively tend to an underestimation of about 10%,

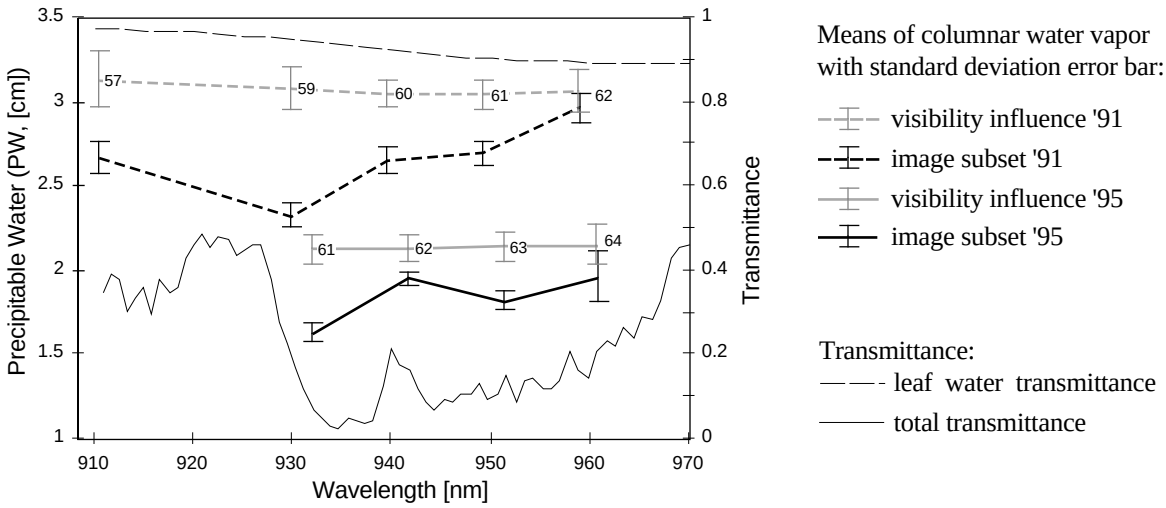

Figure 7: Qualification results for APDA techniques with one measurement channel for 1991 and 1995 data. The obvious underestimation in the channels 59 (1991) and 61 (1995) can be explained with the steep total transmittance slope.

which could be explained by the position of the 930 nm band in the steeply falling water vapor absorption slope at this wavelength. On the other side of the absorption band (channels 62 and 64) a higher estimation is observed. This pattern can either come from the (increased) liquid leaf water absorption at this wavelength or from the unknown spectral channel position shift. The error induced by aerosols is nearly twice as large for methods with measurement channels in the slope of the band than for those in the center. Hence, measurement channels located in the slope, i.e. beside the absorption maximum, should only be used with caution.

The PW estimates for different reference channel combinations (at constant measurement channels) were found to be within $\pm$ 2% over the subset. Furthermore the distance from the central measurement channel and the total number of reference channels had an only marginal influence on the retrieval results. It was even observed, that the qualifiers get worse above 5 reference channels. Therefore only methods with up to four reference channels were further considered.

The APDA(60,61;54,67) method was finally selected for application to the images of 1991 and the ADPA(61,62;54,55,68,69) for 1995 data. The estimated RMS errors due to an aerosol variation between visibilities of 40 km and 10 km at ground level was for both situations below 0.09 cm (PW), which is a relative error of 2 to 3 %. The image subset standard deviations for 1995 were mainly improving against 1991 data, because of the improved SNR values. The relative error reduced from 2.5 to 2 % (down to 0.04 cm PW). The theoretical total error of the retrieval is estimated to be below 5% (aerosol error + image noise error) on the column water vapor amount.

6.3 Optimization of the Atmospheric Path Radiance Term

The atmospheric path radiance term $L_{atm,i}$ in the APDA equation (8) is highly dependent on the atmospheric composition and the terrain elevation. The simulation with the MODTRAN3 code can therefore never be absolutely correct. To find an improved correction term, the one given by MODTRAN3 over zero albedo can be stretched by a constant factor a, so that

$$L_{atm,i} = L_{atm,i,MOD3}\left(1 - \frac{g_i}{\max_{i=[N_1:N_2]}(g_i)}(1-a)\right), \quad \text{where } g_i = \frac{L_{atm,i}(dry)}{L_{atm,i}(wet)} - 1 \tag{18}$$

where $L_{atm,i,MOD3}$ is the basic atmospheric path radiance, as derived from MODTRAN3 for channel i,

ranging from the first look up table channel N_1 to the last N_2. A channel weighting factor g_i (which describes the influence of water vapor changes on $L_{atm,i}$) is found from the ratio between a maximal and a minimal atmospheric path radiance under 'wet'($L_{atm,i}(wet)$) and 'dry' ($L_{atm,i}(dry)$) simulated conditions. The weighting factor g_i is then normalized between 0 and 1, so that the channel with the highest path radiance change between 'wet' and 'dry' gets a g-weighting of 1, whereas no changes are assigned to $g_i = 0$.

To find the channel independent stretch factor a for one specific APDA method, the standard deviation of the method results for an image subset is calculated. This term $\sigma(PW)_{sub}$ is minimized by systematically varying the factor a in equation (18) and introducing the stretched pre-correction terms $L_{atm,i}$ into the APDA equation (see figure 5). The thus found LUT stretch factor a is finally used for the processing of the whole image.

7 APPLICATION OF THE APDA TECHNIQUE TO AVIRIS DATA

The methodology described in the previous sections was applied to two AVIRIS scenes:

1) Site: Central Switzerland,'Risch' Date: July 5th, 1991 run 6, scene 1
2) Site: Santa Monica,'Camarillo' Date: May 26th, 1995 run 8, scene 3

7.1 Central Switzerland

The selected differential absorption method for 1991 was applied to the AVIRIS'91 scene of Central Switzerland (Meyer, 1994). The SNR of the '91 data was only one fifth compared to the most recent AVIRIS data. However, this data set is valuable for atmospheric imaging spectrometry because of the extensive simultaneous in-situ measurements of atmospheric trace gases, taken during the Swiss POLLUMET experiment. Various balloon soundings in and near the test region were combined to obtain the actual profile for the date of over flight (July 5th, 1991). The error of these radiosonde measurements is estimated to be $\pm 10\%$. Additionally, the spatial distribution of water vapor was measured by in situ flights of an ultra light aircraft.

The data were georectified with subpixel accuracy by Meyer (1994). The fully height dependent APDA technique could therefore be applied to the mountainous scene. The water vapor retrieval results of the APDA(60,61;54,67) method are shown in figure 2. The highest columnar amounts measured near the shore in the image are about 2.9 cm and the mean column near the shore is 2.85 cm. The integration of the measured water vapor profiles taken from radiosonde data yields a total column of 2.97 cm over the lake level (414 m a.s.l.). This small difference of about 5% between radiosonde data and the quantified AVIRIS values is within the error of radiosonde data in general and also within the error range of the retrieval procedure described above.

The highest concentrations of water vapor (in $[g/m^3]$) are found in the boundary layer (lower troposphere) with an exponential decrease with height. Therefore the spatial water vapor distribution correlates very well with the DTM of the region, because the highest concentrations of water vapor are found in the boundary layer (lower troposphere) with an exponential decrease with height. The difference in terrain height between the highest and the lowest terrain pixel (954 m a.s.l and 414 m a.s.l, respectively) causes a decrease of water vapor column of about 0.9 cm. The same amount is obtained by integrating the radiosonde profile between these two levels, within an error of less than 5%.

The meteorological interpretation of the water vapor distribution in rugged terrain using the calculated images is difficult, because the influence of the terrain overrides real horizontal changes in water vapor concentrations. To reduce this terrain effect, first an average 'ideal' water vapor distribution map based on the digital elevation model and the average total columnar water vapor contents $\overline{PW_h}$ over the height levels h is calculated:

$$\overline{PW_h}(x,y) = \text{mean}(PW(x,y))|_{h(x,y)} \tag{19}$$

For each pixel (x,y) of the elevation h the difference ΔPW between the pixelwise calculated water vapor (PW) and the 'ideal' water vapor distribution is the terrain independent relative column water vapor:

$$\Delta PW(x,y) = PW(x,y) - \overline{PW_h}(x,y) \tag{20}$$

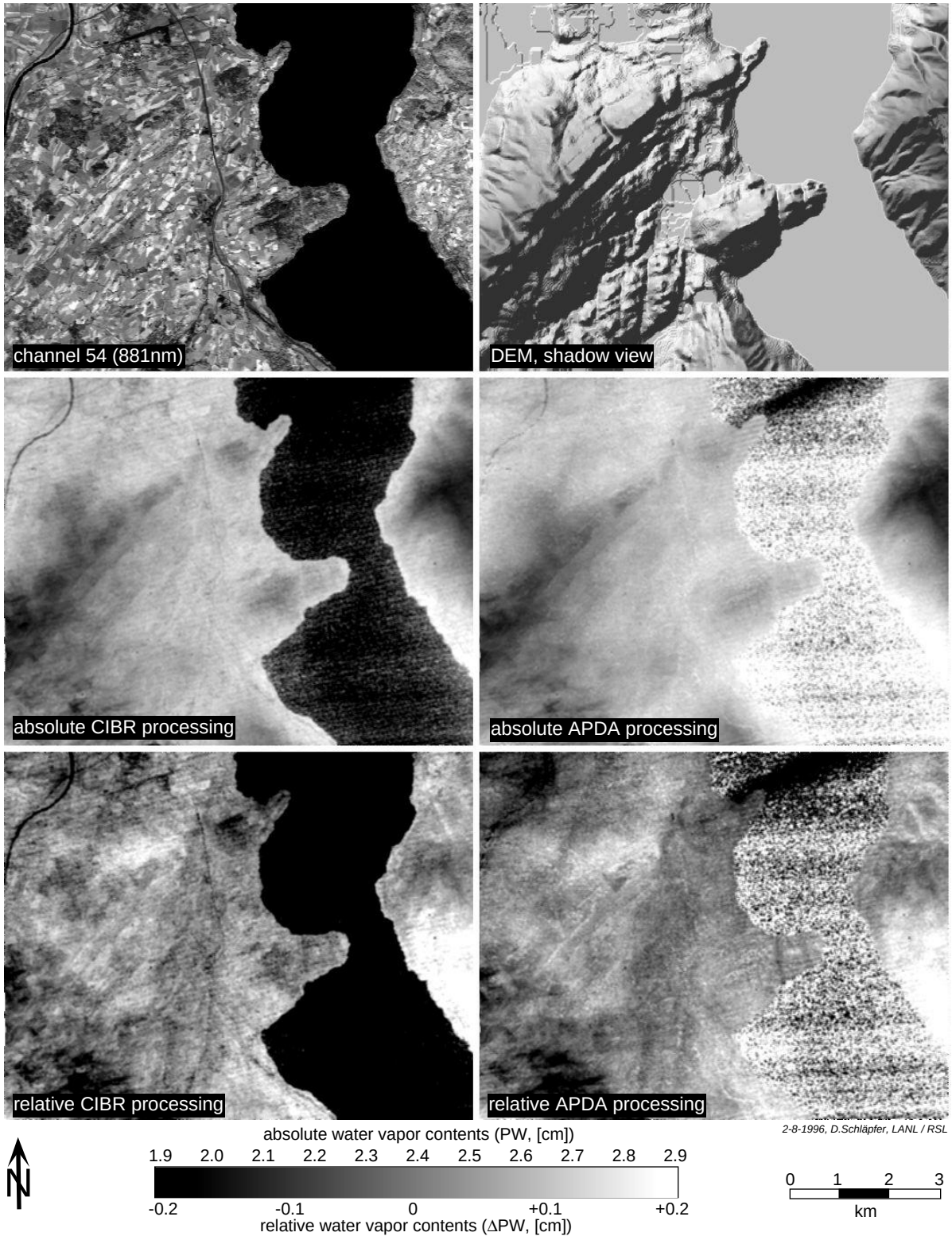

Figure 8: Processing of 1991 AVIRIS data, Central Switzerland, using channels 54,60,61 and 67. Upper right: Near infrared channel 54, upper left: DEM used for the geocoding of the image. Middle images: Absolute water vapor retrieval with CIBR (left) and APDA technique (right). Lower images: Relative water vapor distribution (ΔPW) resulting from CIBR (left) and APDA (right).

The resulting terrain adjusted differential water vapor maps for LIRR and APDA calculation are shown in figure 8. In the uncorrected image, obvious underestimations over the relatively dark forests can be observed, as already described by Gao and Goetz (1990). If the atmospheric pre-correction is applied, a significant improvement is achieved. Most of the errors caused by variations of the background reflectance disappear, leading to a better estimate of relative water vapor concentrations. Even over the lake the strong underestimation in the CIBR processing is strongly reduced by the APDA technique. In the uncorrected distribution maps, the influence of the complex terrain overrides such background effects leading to the erroneous conclusion, that no atmospheric pre-correction were necessary.

7.2 Scene over Camarillo, CA

The application of the APDA technique on the 1995 data showed the unexpected effects of edge-enhancement along the borders of the agricultural fields (see figure 9 upper right images). Since cast shadows in irrigation channels and from plants would not show this phenomenon in a systematic way, a sensor inherent effect is supposed. According to Chrien (1996) the new AVIRIS focal plane is equipped with erroneous amplifiers which cause bright areas bounded by dark areas to appear somewhat delayed. The delay increases with the magnitude of changing signal. Since the reference channels have more than twice the signal of the measurement channels, their delay was significantly higher. To correct for this effect, a pixel shift between single channels was assumed (already before we got notice about the above AVIRIS hardware problem). A procedure to detect sub-pixel shifts (Varosi, 1994) was run over the channels used in the water vapor retrievel algorithm. This analysis, which maximizes the correlation between the single channels, showed that the used reference channels (# 54,55,56,68,69,70) were shifted across the flight direction by about 0.15 pixels to the measurement channels (# 60,61,62,63), whereas in flight direction nearly no shift was detected. All relevant channels were then registered by shifting them by the calculated sub-pixel shifts, using bilinear interpolation. The corrected water vapor images were significantly improved compared to the uncorrected images.

Figure 9 shows the effects of pixel shift correction and atmospheric pre-correction: The borders of the fields remain enhanced, even if the APDA technique is applied (upper right images). Only a pixel shift correction removes this artifact. When doing the traditional differential absorption technique, high impacts of the background characteristics are reported, with underestimations over dark surfaces (lower left image). After the atmospheric pre-correction most of this impact disappears (lower right image). The resulting water vapor distribution is much less biased by the land use features of the ground than the previous water vapor calculation (the smoother appearance is not a filtering effect but only due to the applied correction steps!).

The calculation includes channel 61, because of its qualitative improvement to the resulting image. Since this channel was shown to introduce underestimations of 5 to 8 % (see section 6.2, figure 7) against methods without that measurement channel, the quantification was raised by 6 %. The range of the water vapor concentrations is then within about 1.7 to 2.0 cm, and even fine variations over the plane between 1.8 and 1.9 cm can be observed in the shift corrected APDA image. This accuracy can not be achieved with the CIBR or LIRR technique, where background effects override the signal of the water vapor. In the final image there are still small ground reflectance caused effects, which show that there is opportunity to improve the water vapor retrieval results by a better atmospheric pre-correction or possibly by using spectral classification techniques.

8 CONCLUSIONS

An efficient technique to determine the amount of columnar water vapor has been derived from a modified radiative transfer equation. The technique seems to work much better than the current CIBR techniques which neglect the effects of path radiance. It is shown how the CIBR and APDA behave over dark, bright, and spectrally variable backgrounds. A large number of mineral, man-made, and simulated vegetation spectra were used, and the relative water vapor error lies within $\pm 5\%$ for most reflectance spectra. This accuracy is sufficient for current applications since sensor calibration and modeling errors are estimated to have similar relative errors. It was shown that the introduced atmospheric pre-corrected differential absorption (APDA) technique allows the measurement of spatial water vapor distributions even over flat areas with strong

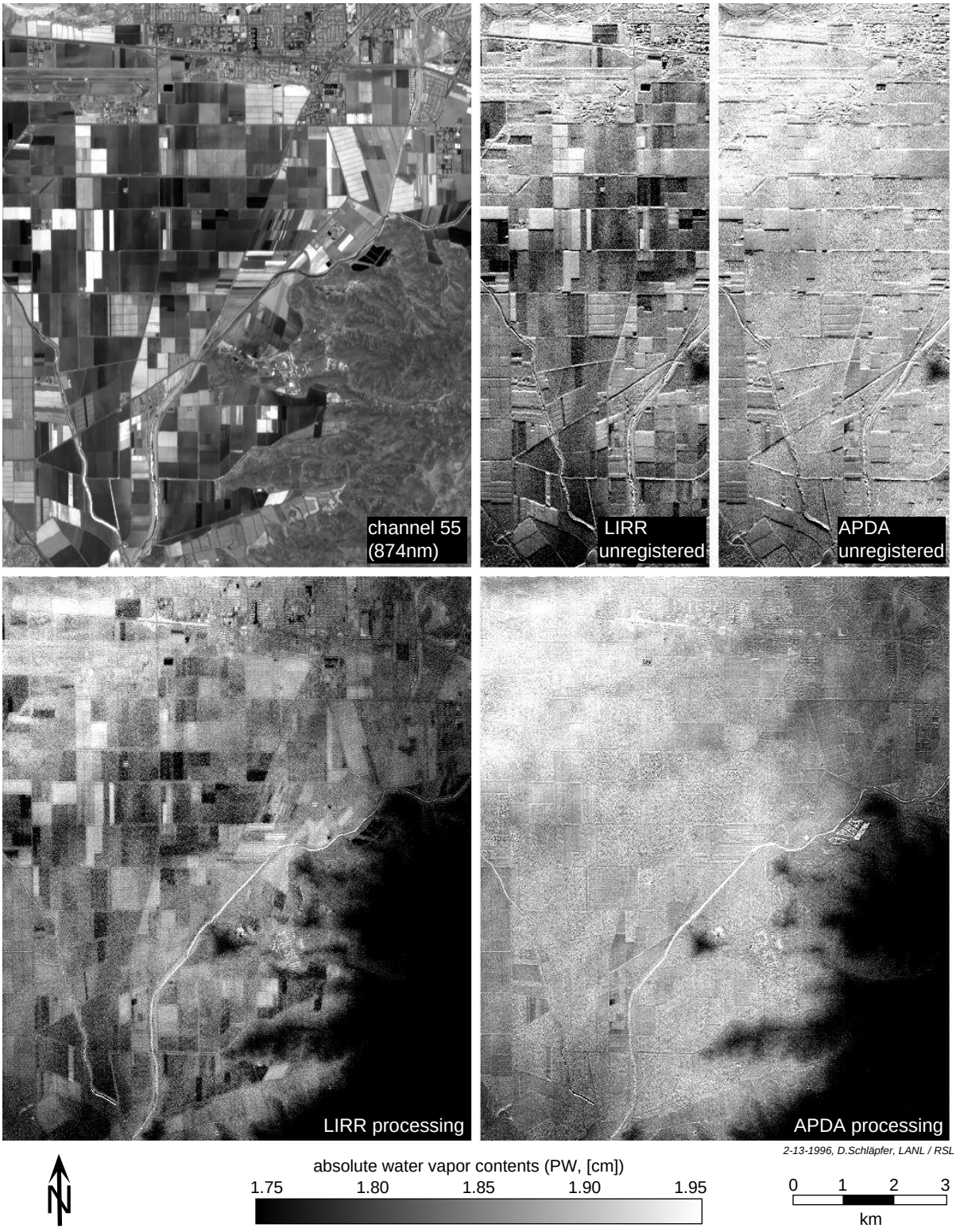

Figure 9: Processing of 1995 AVIRIS data, Camarillo, using channels 54,55,61,62,68 and 69. Upper left: raw channel 54, upper right: unregistered LIRR resp. ADPA processing (no pixel shifting applied). Lower left: LIRR processing (after pixel shift registration), Lower right: APDA processing.

background reflectance variations. Prior to the application of the APDA technique a quantitative method of channel selection yielded ranked sets of channels, and a large set of retrieval methods were evaluated using an exclusion and ranking process. This combination of optimized channel selection, method evaluation and the APDA technique made it possible to achieve the significant improvement compared to traditional differential absorption techniques.

The distribution with terrain height for 1991 data was very similar to the profile measured by radio sondes, although the image was calibrated by the integrated total water vapor column (the slope of the water vapor profile has a negligible effect on the columnar results). Hence, the used methodology has the potential to derive water vapor profiles from the boundary layer, using the digital elevation model.

In future work such profiling methods will be searched and three dimensional modeling of the water vapor distribution in valleys will be tried. A challenge remains to determine water vapor over dark surfaces such as water or shadowed areas, since the path radiance is now the only quantity containing information about the atmosphere. This complementary measurement of water vapor will only be possible with further improvements of the methodology. Such methods will differ essentially from the differential absorption and nonlinear curve fitting techniques. The most promising approaches are the improvement of the atmospheric pre-correction by introducing an iterative water vapor retrieval process or the application of classification algorithms and spectral databases. More work is also needed to retrieve water vapor over rough terrain. The presented techniques may also be useful to retrieve other gases such as CO_2 and O_2.

9 ACKNOWLEDGEMENTS

The following institutions, foundations and persons are greatly acknowledged: The Swiss National Science Foundation, NASA's and LANL's Remote Sensing Science Programs and the US Department of Energy for the financial support of the project, the AVIRIS group at the JPL Pasadena for providing the AVIRIS-images, Los Alamos National Laboratory (LANL) and the Remote Sensing Laboratories (RSL) Zurich for their facilities. We acknowledge many fruitful technical discussions with and work done by Veronique Carrére (ISPRA, Italy) , James Theiler(LANL), and Bill Clodius (LANL).

10 References

Abreu L.W., Chetwynd, J.H, Anderson, G.P. and Kimball, L.M. (1995), MODTRAN 3 Scientific Report, Draft Preprint, Geophysics Laboratory, Air Force Command, US Air Force, Hanscom AFB, Ma, USA.

Berk, A., Bernstein, L.S., and Robertson, D.C. (1989), MODTRAN, A Moderate Resolution Model for LOWTRAN 7. Geophysics Laboratory, Air Force Command, US Air Force, Hanscom AFB, MA, USA.

Borel, C.C., and Gerstl S.A.W. (1994) Non-linear Spectral Mixing Models for Vegetative and Soil Surfaces, Remote Sens. of the Environment, 47:403-416.

Borel, C.C, and Schläpfer, D., (1996), Atmospheric Pre-Corrected Differential Absorption Techniques To Retrieve Columnar Water Vapor: Theory, Proceedings of the 6th JPL Airborne Earth Science Workshop, JPL, Pasadena (in press)

Bruegge, C.J., Conel, J.E., Margolis, J.S., Green, R.O., Toon G., Carrére, V., Holm, R.G. and Hoove,r G., (1990), In-situ Atmospheric Water-Vapor Retrieval in Support of AVIRIS Validation, SPIE Vol. 1298 Imaging Spectroscopy of the Terrestrial Environment, pp 150 - 163.

Carrére, V., and Conel, J.E., (1993), Recovery of Atmospheric Water Vapor Total Column Abundance from Imaging Spectrometer Data around 940 nm - Sensitivity Analysis and Application to Airborne Visible/ Infrared Imaging Spectrometer (AVIRIS) Data, Remote Sensing of Environment, Nr. 44 , pp 179 - 204.

Frouin, R., Deschamps, P.-Y, and Lecomte, P. (1990), Determination from Space of Atmospheric Total Water Vapor Amounts by Differential Absorption Near 940 nm: Theory and Airborne Verification, Journal of Applied Meteorology, Vol. 29, American Meteorological Society, pp 448 - 459.

Gao, B.-C., and Goetz, A.F.H.(1990a), Determination of Total Column Water Vapor in the Atmosphere At

High Spatial Resolution from AVIRIS Data Using Spectral Curve Fitting and Band Ratioing Techniques, SPIE Vol. 1298, Imaging Spectroscopy of the Terrestrial Environment, pp 138 - 149.

Gao, B.-C., and Goetz, A.F.H. (1990b), Column Atmospheric Water Vapor and Vegetation Liquid Water Retrievals from Airborne Imaging Spectrometer Data, Journal of Geophysical Research, Vol. 95, No. D4, pp 3549 - 3564.

Gao, B.-C., Heidebrecht, K.B. and GOETZ A.F.H. (1993), Derivation of Scaled Surface Reflectance from AVIRIS Data , Remote Sensing of Environment, Nr. 44, New York, pp 165 - 178

Green, R.O., Carrére, V., and Conel, J.E.(1989), Measurement of Atmospheric Water Vapor Using the Airborne Visible/Infrared Imaging Spectrometer, Am. Soc. Photogram. and Remote Sensing, Workshop Image Processing, Sparkes, Nevada, 23-26 May.

Grove, C.I., Hook, S.J., and Paylor, E.D.(1992), Spectral Reflectance of Minerals 0.4 to 2.5 Micrometers, JPL Publication 92-2.

Jacquemoud, S., Ustin, S.L., Verdebout, J., Schmuck, G., Andreoli, G. and Hosgood, B.(1995),PROSPECT REDUX, Proceedings AVIRIS Workshop, Pasadena, January.

Kaufman, Y.J., and Gao, B.-C., (1992), Remote Sensing of Water Vapor in the Near IR from EOS/MODIS. IEEE Transactions on Geoscience and Remote Sensing, Vol. 30, No. 5, pp 871 - 884

Kruse, F.A. (1992), unpublished data, IUGS Special Publication.

Meyer, P. (1994), A Parametric Approach for the Geocoding of Airborne Visible/Infrared Spectrometer (Aviris) Data in Rugged Terrain, Remote Sensing of Environment, Vol. 48, pp 1-25

Middleton, W.E.K. (1952), Vision Through the Atmosphere, University of Toronto Press.

Schläpfer, D., Keller, J., and Itten, K.I., (1995), Imaging Spectrometry of Tropospheric Ozone, New Methods of Channel Selection , presented at IGARSS'95, Florence, separatum (not in proceedings), p 3

Schläpfer, D., Keller, J., and Itten, K.I., (1996a), Imaging Spectrometry of Tropospheric Ozone and Water Vapor, Proceedings of EARSeL Workshop (in press), Basel (Switzerland), p 8

Schläpfer, D., Borel, C.C., Keller, J., and Itten, K., (1996b), Atmospheric Pre-Corrected Differential Absorption Techniques to Retrieve Columnar Water Vapor: Application to AVIRIS 91/95 Data, Proceedings AVIRIS Workshop (in press), Pasadena (CA).

Varosi, F, (1988-1995), Varosi's General Purpose IDL Code Library (vlib), Mail Code 685, ftp:// idlastro.gsfc.nasa.gov /contrib/varosi, NASA/Goddard Space Flight Center, Greenbel MD.

Vermote, E., Tanré, D., Deuzé, J.L., Herman, M. and Morcette, J.J., (1994), Second Simulation of the Satellite Signal in the Solar Spectrum, 6S User Guide Version 0, NASA-Goddard Space Flight Center, Greenbelt, USA, P 182.